R. I. Leine
e-mail: r.i.leine@tue.nl

D. H. van Campen

Department of Mechanical Engineering,
Eindhoven University of Technology,
P.O. Box 513, 5600 MB Eindhoven,
The Netherlands

W. J. G. Keultjes

Shell International Exploration
and Production b.v.,
Volmerlaan 8, P.O. Box 60, 2280 AB Rijswijk,
The Netherlands

Stick-slip Whirl Interaction in Drillstring Dynamics

This paper attempts to explain the complicated behavior of oilwell drillstring motion when both torsional stick-slip and lateral whirl vibration are involved. It is demonstrated that the observed phenomena in experimental drillstring data could be due to the fluid forces of the drilling mud. A Stick-slip Whirl Model is presented which consists of a submodel for the whirling motion and a submodel for the stick-slip motion, both as simple as possible. The Stick-slip Whirl Model is a simplification of a drillstring confined in a borehole wall with drilling mud. The model is as simple as possible to expose only the basic phenomena but is discontinuous. Bifurcation diagrams of this discontinuous model for varying rotation speeds reveal discontinuous bifurcations. The disappearance of stick-slip vibration when whirl vibration appears is explained by bifurcation theory. The numerical results are compared with the experimental data from a full-scale drilling rig. [DOI: 10.1115/1.1452745]

1 Introduction

Deep wells for the exploration and production of oil and gas are drilled with a rock-cutting tool driven from the surface by a slender structure of pipes, called the drillstring (Fig. 1). Drillstring vibrations are an important cause of premature failure of drillstring components and drilling inefficiency. Stick-slip vibration causes violent torsional vibration of the drillstring and whirl leads to lateral vibrations with large amplitudes. Extensive research on this subject has been conducted for the last four decades, both theoretically [1–7] and experimentally [8–12]. Whirling motion of a drill collar section has been studied by [1,2,7]. Models for torsional stick-slip motion of a drillstring were presented in [2] and extensively analyzed by [3,6]. Most of the experimental investigations were only based on field measurements recorded at the surface [8–11]. Stick-slip vibrations can indeed be detected from the surface, at least in a straight well, but detailed information about the mechanism downhole cannot be obtained. Downhole measurements, briefly presented in this paper, reveal stick-slip vibration coexisting with whirl vibration. Uncertainty exists on the downhole mechanism which determines whether stick-slip or whirl will be prevalent. This paper presents a low-dimensional dynamical model, describing stick-slip and whirl in its most elementary form. This model aims at explaining the basic nonlinear dynamics phenomena observed in downhole experiments. The model system is analyzed with the methods presented in [13–16] which are shortly summarized in Appendix A. It is demonstrated that the model system exhibits several types of discontinuous bifurcations. We will discuss in Section 10 the possible merits of this paper to the insight into drillstring vibration.

Dynamical problems of drillstrings are analyzed in industry using linear models for critical rotary speeds and buckling loads and large finite element models [2], which give quantitative information and can help to give practical recommendations to circumvent drilling problems. The finite element models are however so complex (nonlinear large displacement, finite rotation, many degrees of freedom) that it is very difficult to obtain insight why certain vibrational phenomena occur. Small low degree of freedom models, which can be analyzed with analytical methods, can provide (to some degree) qualitative insight in a specific complex phenomenon occurring in reality. The aim of the Stick-slip Whirl Model, proposed in this paper, is to explain qualitatively the ob-

served phenomenon of stick-slip to whirl transitions in a real drillstring. The model is kept as simple as possible and does not pretend to give any quantitative information.

The principles of oilwell drilling are first briefly explained in Section 2. Downhole measurements, which reveal stick-slip motion and whirl in a drillstring, are presented in Section 3. A simple mathematical model for the investigation of stick-slip and whirl is constructed and analyzed in Sections 4 to 9. The theoretical and numerical results will be compared with results obtained from measurements in Section 10.

2 Principles of Oilwell Drilling

Oil and gas wells are predominantly drilled using rotary drilling. The basic elements of a rotary drilling system are shown in Fig. 1. A rotary drilling system creates a borehole by means of a rock-cutting tool, called a bit. The oldest type of rotary bit is the roller-cone bit which essentially comprises three metal rollers covered with hard steel teeth that crush the rock. An alternative type of bit is the PDC (Polycrystalline Diamond Compact) bit consisting of a steel body with inserts made of artificial diamond and tungsten carbide. The energy to drive the bit is generated at the surface by a motor with a mechanical transmission box. Via the transmission the motor drives the rotary table: a large disc that acts as kinetic energy storage. The medium to transport the energy from the surface to the bit is formed by a drillstring, mainly consisting of drill pipes: slender tubes, about 9 m (30 ft.) long, coupled with threaded connections, having a typical outside diameter of 127 mm (5 in.) and a wall thickness of 9 mm. However, smaller (e.g. 3.5 in.) and larger (6.5 in.) drill pipe diameters are also used.

The lowest part of the drillstring, the Bottom-Hole-Assembly (BHA), consists of thick-walled tubulars, called drill collars. Dependent on the diameter of the hole, these drill collars usually have an inner diameter of 2.5–3 in. (64–76 mm) and an outer diameter of 4.75 in.–9.5 in. (120–240 mm). The BHA can be several hundreds of meters long, and often contains dedicated downhole tools. The drill collars in the BHA are kept in position by a number of stabilizers, which are short sections with nearly the same diameter as the bit.

The drilling process requires a compressive force on the bit of some $10^4 - 10^6$ N. This dynamic force is commonly denoted as Weight On Bit (WOB), although force-on-bit would be a more appropriate name. The entire drillstring is suspended by a hoisting system, consisting of a travelling block with hook, drilling line and winch. The drillstring rests with the bit on the bottom of the hole and is pulled at the hook by a force called the hookload. The
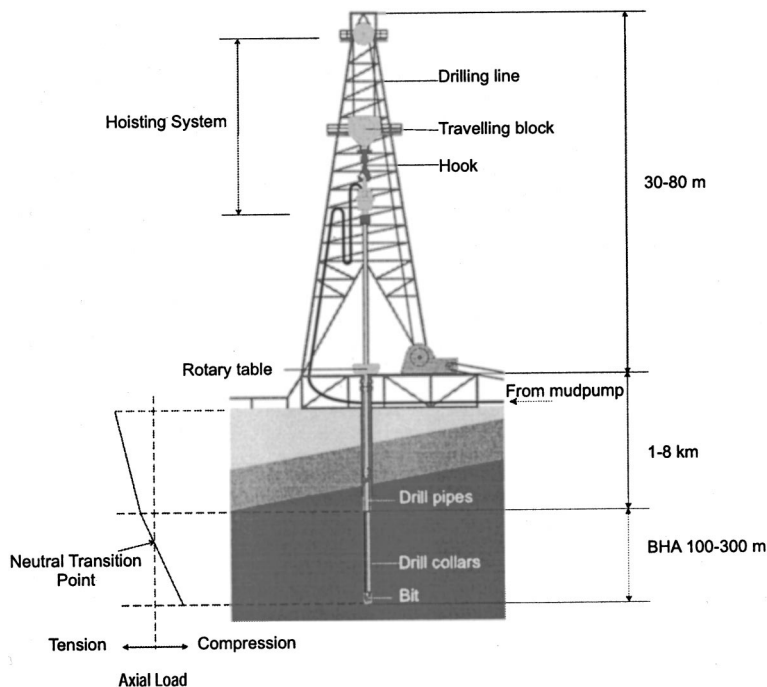
Fig. 1 Drilling rig

hookload ensures that the drill pipe is kept in tension to avoid buckling. The graph at the left of Fig. 1 shows the axial force as a function of the position along the borehole. While the drill pipes run in tension, the BHA is partly loaded in compression. The combined loading of the BHA in axial and torsional direction can cause buckling of the BHA. Buckling of the BHA is prevented by the large wall thickness of the drill collars and the placement of stabilizers. An ideal stabilizer would provide a ''hinge'' boundary condition for the lateral movements of the drillstring. The critical buckling load rises due to the additional supports of the stabilizers.

Torque is transmitted from the rotary table to the drillstring. The torque required to drive the bit is referred to as the Torque On Bit (TOB).

A fluid called mud is pumped down through the hollow drillstring, through nozzles in the bit and returns to the surface through the annulus between the drillstring and the borehole wall. The mud compensates the pressure in the rock, lubricates and removes the rock cuttings from the hole.

The drilling process is steered by the hookload, the rotary table speed at the surface (the angular velocity of the top end of the drillstring) and the flow rate of the mud. The downward speed of the drillstring gives an accurate measure of the rate of penetration (ROP). The standpipe pressure (the pressure in the flowline at the top of the drillstring) indicates the total pressure drop in the drillstring and annulus. The ROP and standpipe pressure indicate the progress and state of the drilling process which are interpreted by drilling engineers to adjust the steering parameters.

The drillstring undergoes various types of vibration during drilling [6]

• Axial (longitudinal) vibrations, mostly due to the interaction between drilling bit and the hole bottom. In its extreme form, when the bit can lose contact with the hole bottom, this vibration is called ''bitbounce''.
• Bending (lateral) vibrations, often caused by pipe eccentricity, leading to centripetal forces during rotation, named as drillstring whirl:

- **forward whirl**: the rotation of a deflected drill collar section around the borehole axis in the same direction as it rotates around its axis.
- **backward whirl**: a rolling motion of the drill collar or the stabilizer over the borehole wall in opposite direction as it rotates around its axis.
• Torsional (rotational) vibrations, caused by nonlinear interaction between the bit and the rock or the drillstring with the borehole wall, named as
- **stick-slip vibration**: the torsional vibration of the drillstring characterized by alternating stops (during which the BHA sticks to the borehole) and intervals of large angular velocity of the BHA.
• Hydraulic vibrations in the circulation system, stemming from pump pulsations.

These vibrations are to some degree coupled: e.g. the interaction between TOB and WOB will link the axial vibrations to the torsional vibrations.

3 Downhole Measurements

In the late 1980s the Institut Français du Pétrole designed the Trafor system, a research tool to measure downhole and surface data to improve knowledge about drillstring dynamics. The Trafor system consists of a downhole measurement device, called the Télévigile, and a surface measurement device known as the Survigile. The signals of the Télévigile and Survigile are gathered by a computer and synchronized. The great merit of the Trafor system is the ability to measure both downhole and surface data at real-time. Pavone and Desplans [12] give a description of the Trafor system. The Télévigile is basically a tube much like a normal drill collar, but equipped with sensors that measure Weight On Bit, downhole torque, downhole accelerations in three orthogonal directions and downhole bending moments in two directions. Three magnetic field sensors, known as magnetometers, measure a projection of the earth magnetic field in three orthogonal directions co-rotating with the Télévigile.

The measurements reported in this section were recorded at a full-scale research rig. The well is nearly vertical and about
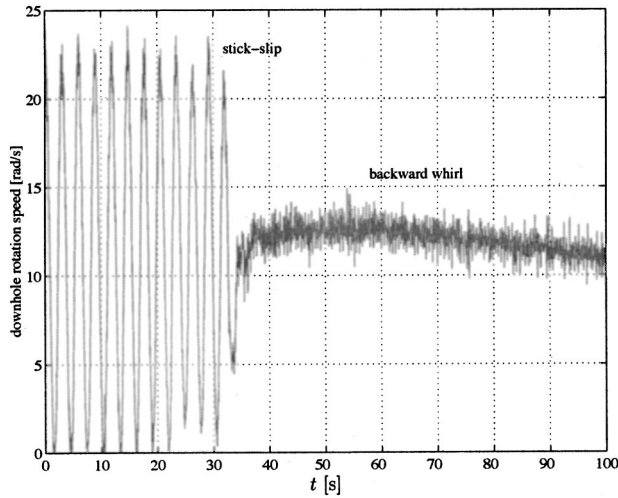
Fig. 2 Measured downhole angular velocity versus time

Fig. 4 Measured downhole bending moment versus surface angular velocity; sweep-up followed by sweep-down

1080 m deep. Various tests with different WOB and angular velocity of the rotary table were conducted. A few tests are used for this paper, all conducted with the same drillstring setup. The drillstring consisted of 5 in. drill pipe, 8 in. drill collars and a 12 1/4 in. roller-cone bit.

Figure 2 shows a time history of the downhole angular velocity, calculated from the magnetometer signals. The angular velocity at the surface ω, WOB and other parameters were almost kept constant during the experiment. The drillstring clearly performs stick-slip motion for $t<35$ s. At $t=35$ s the stick-slip motion suddenly disappears and backward whirl is prevalent for $t>35$ s. Backward whirl can be recognized by studying the bending moments (see Fig. 4). The stick-slip motion is caused by the dry friction between the BHA and the rock. The friction is due to the drilling bit, which cuts the rock, but also due to the stabilizers, which have contact with the borehole wall. The friction curve of the part of the BHA beneath the Télévigile, relating the torque to the downhole angular velocity, could be reconstructed from the measurements (Fig. 3). The torque on the Télévigile consists of the friction torque of the bit, the torque created by contact (if present) of the drill collar beneath the Télévigile with the borehole wall and by the viscous torque of the drilling mud. During the stick-slip motion the part of the friction curve is traversed with the negative slope. The negative slope of the friction curve causes steady rotation of the drillstring to be unstable, which induces the stick-slip motion. At the
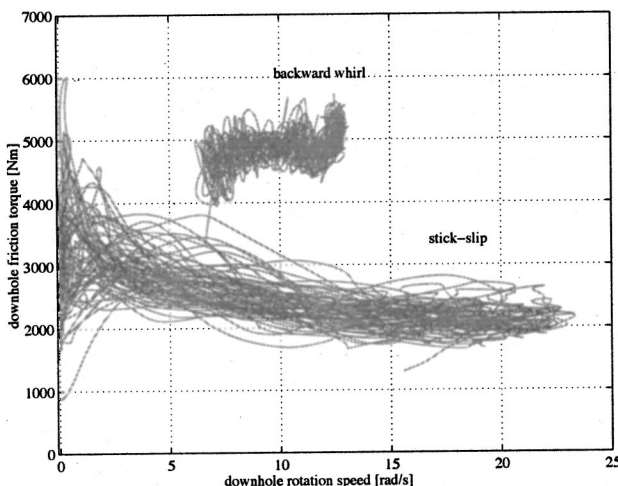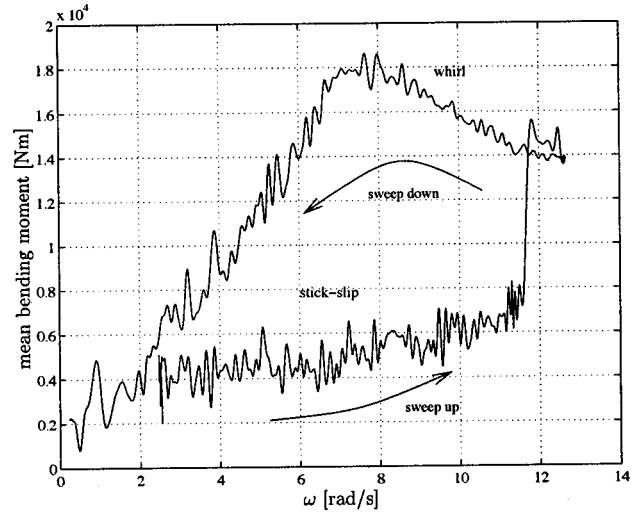

Fig. 3 Measured downhole friction curve

transition to whirl, a switch is made to another part of the friction curve with a higher value of friction and a slightly positive slope. The drillstring is not deflected in lateral direction during stick-slip motion. Consequently, the torque on the Télévigile is during stick-slip motion mainly due to the friction torque on the bit. The whirl motion has been identified as being backward whirl caused by rolling of a drill collar section over the borehole wall (with a small amount of slip). The drillstring must consequently be deflected during whirl motion. The torque on the Télévigile will be higher during whirl motion due to the additional torque created by the contact between drill collar and borehole wall and increased drag forces of the mud on the whirling drill collar. This additional torque increases with increasing angular velocity. This would account for the higher torque and slightly positive slope of the friction curve during whirl motion. The slightly positive slope causes the constant rotation to be stable which prevents stick-slip motion as is observed in Fig. 2.

Figure 4 shows the mean bending moment measured by the strain gauges in the Télévigile versus the prescribed angular velocity at the surface ω. During this experiment, the value of ω was varied with a sweep-up followed by a sweep-down (300 s each). The mean bending moment is to some extent a measure for the radial displacement of the drillstring (assumed that the drill collar section with the Télévigile is bent in its first bending mode). The system was first in stick-slip motion with a low value of the mean bending moment (consistent with an undeflected drillstring) at low ω. As ω is increased the mean bending moment increases slightly but at $\omega=11.5$ [rad/s] the motion switches from stick-slip to whirl and the mean bending moment jumps to a higher value, indicating a large radial deflection of the drillstring. The sweep-up test reaches its maximum at $\omega=12.5$ [rad/s] after which ω is decreased. The drillstring remains in whirl motion down to $\omega=2$ [rad/s]. The bending moment during whirl motion is not constant for varying ω. The part with positive slope for $2<\omega<7$ [rad/s] is consistent with an increasing radial deflection for increasing ω. At $\omega=7$ [rad/s] the Télévigile probably touches the borehole wall and for increasing values of ω, a larger part of the drillstring will become in contact with the borehole wall which decreases the bending moment. We conclude from Fig. 4 that stick-slip and whirl can coexist for an interval of rotary table speed ω. Combined stick-slip whirl motion, however, in which the drillstring performs stick-slip motion with a large radial deflection, is not observed.

The mechanism downhole, which causes the transition from stick-slip to whirl and vise-versa, is not satisfactorily understood.

The transition from stick-slip to whirl is presumably caused by an interaction between bending and torsion which destabilizes the concentric position of the drillstring for high values of ω. Possible ways of interaction can be caused by

- Drillstring eccentricity. This causes the drillstring to whirl violently only in the neighborhood of the bending critical eigenfrequency. The drillstring would not whirl for very high values of ω, contrary to what has been observed from the measurements.
- Gyroscopic effects. They are negligible because the clearance between drillstring and borehole is much smaller than the length of the drillstring.
- Anisotropic bending stiffness of the drillstring. This causes the drillstring to whirl in a small interval of ω which is inconsistent with the measurements.
- Fluid mud forces. They destabilize the concentric position of the drillstring for ω-values higher than a critical value consistent with measurements.

Insight into the mechanism downhole and the possible interaction between bending and torsion can be obtained by studying a simplified model of the drillstring. In the next sections we will study whether fluid forces of the drilling mud can explain the observed phenomena. A low-dimensional model will be analyzed with both torsional and lateral degrees of freedom in a fluid. This small model will be discontinuous of Filippov-type and shows a complicated dynamical behavior. Bifurcations in Filippov systems were investigated in [15,16]. The results of [15,16] will be of use to partly explain the complicated dynamical behavior of the model.

4 Modeling of Stick-slip Whirl Interaction

A simple model for the whirling motion of a drill collar section has been developed by Jansen [1,2] and has been further analyzed by Van der Heijden [7]. A simple model to describe the torsional stick-slip motion of a drillstring was presented in [2] and extensively analyzed by Van den Steen [6] and in [3].

In the following sections we will develop a model which can describe the combined whirl and stick-slip motions in their most elementary form, under influence of fluid forces. The model consists of a submodel for the whirling motion, called the *Whirl Model*, and a submodel for the stick-slip motion, called the *Stick-slip Model*. The full model will be named the *Stick-slip Whirl Model*. Elementary whirling can be described by at least 2 lateral

degrees of freedom and stick-slip motion by one torsional degree of freedom. The Stick-slip Whirl Model has therefore 3 degrees of freedom. The Stick-slip Whirl Model is a simplification of a drillstring confined in a borehole wall with mud.

The interaction between torsional vibration and whirl of a rotor was already studied in [17,18] but a dry friction torque on the rotor and fluid forces were not considered.

We consider a rigid disk (which models the BHA) at the end of a massless flexible shaft (the drill pipe) as is depicted in Fig. 5(a). The shaft and disk are confined in a stator (the borehole) filled with fluid (drilling mud). The upper end of the shaft is driven with constant rotation speed ω (constant speed of the rotary table). The shaft is subjected to bending and torsion with bending stiffness k and torsion stiffness k_φ. The disk with mass m and inertia J is attached to the lower end of the shaft. The displacement of the geometric center of the disk is denoted by x and y in the stationary coordinate system or by the polar coordinates r and α (see Appendix B). The disk is twisted with an angle φ with respect to the upper end of the shaft and with an angle ϕ with respect to the fixed world

$$\phi = \omega t + \varphi. \qquad (4.1)$$

On the disk or *rotor* acts a friction torque T_f (the Torque On Bit). The lateral motion of the disk is constrained by the *stator*. The rotor has a radius R and the stator a radius R_b. Contact is made when the radial (lateral) displacement of the rotor r equals R_c, where $R_c = R_b - R$ is the clearance.

5 Fluid Forces

The fluid forces on the drillstring are extremely complicated as the fluid motion is nonstationary and possibly turbulent. However, analytical results are available for a constantly rotating rotor in a stator for small clearance and small lateral displacement ($R_c \ll R$ and $r \ll R$) [19,20]. As a first approximation we will use these analytical results for nonstationary motion of a rotor which is confined in a large stator for arbitrary lateral displacements. The fluid force equations given in [19,20] are
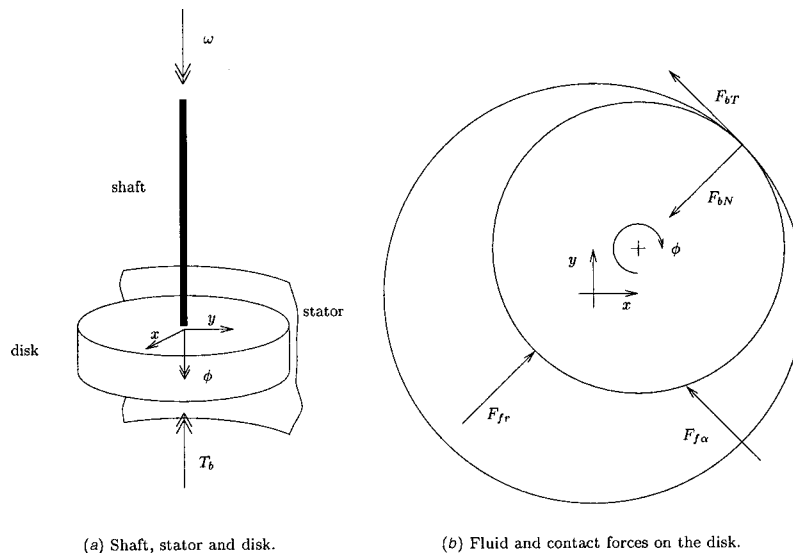

(a) Shaft, stator and disk.   (b) Fluid and contact forces on the disk.

Fig. 5 Stick-slip Whirl Model

$$-\begin{bmatrix} F_{fx} \\ F_{fy} \end{bmatrix} = \begin{bmatrix} m_f & 0 \\ 0 & m_f \end{bmatrix} \begin{bmatrix} \ddot{x} \\ \ddot{y} \end{bmatrix} + \begin{bmatrix} D & \omega m_f \\ -\omega m_f & D \end{bmatrix} \begin{bmatrix} \dot{x} \\ \dot{y} \end{bmatrix}$$

$$+ \begin{bmatrix} \psi_2(r) & 0 \\ 0 & \psi_2(r) \end{bmatrix} \begin{bmatrix} \dot{x} \\ \dot{y} \end{bmatrix} + \begin{bmatrix} -\dfrac{\omega^2}{4} m_f & \dfrac{\omega}{2} D \\ -\dfrac{\omega}{2} D & -\dfrac{\omega^2}{4} m_f \end{bmatrix} \begin{bmatrix} x \\ y \end{bmatrix}$$

$$+ \begin{bmatrix} \psi_1(r) & \dfrac{\omega}{2}\psi_2(r) \\ -\dfrac{\omega}{2}\psi_2(r) & \psi_1(r) \end{bmatrix} \begin{bmatrix} x \\ y \end{bmatrix}, \tag{5.1}$$

where m_f is the added fluid mass and D the fluid friction coefficient.

The fluid forces, depicted in Fig. 5(b), can be transformed to polar coordinates

$$F_{fr} = -m_f\left(\ddot{r} - \dot{\alpha}^2 r - \frac{\omega^2}{4} r + \omega\dot{\alpha} r\right) - (D + \psi_2(r))\dot{r} - \psi_1(r)r \tag{5.2}$$

$$F_{f\alpha} = -m_f(\ddot{\alpha} r + 2\dot{r}\dot{\alpha} - \omega\dot{r}) - \left(\dot{\alpha} - \frac{\omega}{2}\right)(D + \psi_2(r))r.$$

The nonlinear functions ψ_1 and ψ_2 depend on the radial displacement r. It is assumed (following [20]) that these functions are analytic (with $\psi_1(0) = \psi_2(0) = 0$). As a first approximation, only the following symmetric terms will be taken into account:

$$\psi_1(r) = B_1 r^2, \quad \psi_2(r) = B_2 r^2, \tag{5.3}$$

where B_1 and B_2 are constants.

6 Contact Forces

The stator wall will induce normal and tangential forces (Fig. 5(b)) on the rotor if the radial displacement becomes larger than the clearance, $r > R_c$. The normal contact force can be modeled (in its most simple form) to stem from a linear spring with spring stiffness k_b,

$$F_{bN} = \begin{cases} k_b(r - R_c) & r > R_c \\ 0 & r \leq R_c. \end{cases} \tag{6.1}$$

The normal contact force induces a tangential contact force due to dry friction between the rotor and the wall. We assume a constant friction coefficient μ_b. If the relative velocity between the rotor and the stator wall is nonzero, then the tangential contact force is

$$F_{bT} = -\mu_b \operatorname{sign}(v_{\mathrm{rel}}) F_{bN}, \quad v_{\mathrm{rel}} \neq 0, \tag{6.2}$$

with the relative velocity being given by $v_{\mathrm{rel}} = \dot{\alpha} r + \omega R$ (for constant rotation of the rotor). During pure rolling ($v_{\mathrm{rel}} = 0$) the tangential contact force must be between

$$-\mu_b F_{bN} \leq F_{bT} \leq \mu_b F_{bN}. \tag{6.3}$$

The contact forces can be expressed in stationary coordinates as

$$F_{bx} = (-F_{bT}y - F_{bN}x)/r, \quad F_{by} = (F_{bT}x - F_{bN}y)/r. \tag{6.4}$$

The friction due to rotor-stator contact can be treated numerically by making use of the *switch model* [21].

6.1 Torques on the Disk.
We assume that a dry friction torque T_f is acting on the rotor, which only depends on the angular velocity $\dot{\phi}$,

$$T_f = -\operatorname{sgn}\dot{\phi}\,\frac{T_0}{1 + \delta|\dot{\phi}|}. \tag{6.5}$$

This relation between dry friction torque and angular velocity is motivated by Fig. 3. Contact between the rotor and stator induces the contact forces F_{bN} and F_{bT}. The tangential contact force induces a torque on the rotor,

$$T_b = F_{bT}R. \tag{6.6}$$

The fluid forces F_{fr} and $F_{f\alpha}$ of Eq. (5.2) are derived for stationary motion of the rotor $\dot{\phi} = \omega$. We will assume that they also hold for nonstationary motion, $\dot{\phi} \neq \omega$, and we replace ω by $\dot{\phi}$ in Eq. (5.2),

$$F_{fr} = -m_f\left(\ddot{r} - \dot{\alpha}^2 r - \frac{\dot{\phi}^2}{4} r + \dot{\phi}\dot{\alpha} r\right) - (D + \psi_2(r))\dot{r} - \psi_1(r)r \tag{6.7}$$

$$F_{f\alpha} = -m_f(\ddot{\alpha} r + 2\dot{r}\dot{\alpha} - \dot{\phi}\dot{r}) - \left(\dot{\alpha} - \frac{\dot{\phi}}{2}\right)(D + \psi_2(r))r.$$

The fluid forces F_{fr} and $F_{f\alpha}$ act on the rotor but their working lines are through the origin. The force $F_{f\alpha}$ has therefore an arm $-r$ and gives the torque

$$T_d = -F_{f\alpha}r. \tag{6.8}$$

7 Whirl Model

In this section we study only the Whirl Model. We assume the rotor to rotate constantly (no torsional vibration). This allows us to find analytical results for the pure whirling motion, which are equilibria of the Whirl Model in polar coordinates and periodic harmonic solutions in stationary coordinates. Polar coordinates are therefore more convenient for the Whirl Model. The equilibria of the Whirl Model are also equilibria of the total Stick-slip Whirl Model but the eigenvalues of the Stick-slip Model may change the stability.

7.1 Equations of Motion.
The equations of motion for a whirling rotor with fluid and contact forces in stationary coordinates are

$$m\ddot{x} + c\dot{x} + kx = F_{fx} + F_{bx}$$
$$m\ddot{y} + c\dot{y} + ky = F_{fy} + F_{by}, \tag{7.1}$$

where m is the rotor mass, k the lateral bending stiffness and c the lateral bending damping constant. In polar coordinates these equations become

$$m(\ddot{r} - \dot{\alpha}^2 r) + c\dot{r} + kr = F_{fr} - F_{bN}$$
$$m(\ddot{\alpha} r + 2\dot{r}\dot{\alpha}) + c\dot{\alpha} r = F_{f\alpha} + F_{bT}. \tag{7.2}$$

Substitution of the fluid forces of Eq. (5.2) gives

$$m_a(\ddot{r} - \dot{\alpha}^2 r) + (c + D + B_2 r^2)\dot{r} + \left(k - \frac{\omega^2}{4} m_f + m_f\omega\dot{\alpha} + B_1 r^2\right)r$$
$$= -F_{bN}$$
$$m_a(\ddot{\alpha} r + 2\dot{r}\dot{\alpha}) + (c + D + B_2 r^2)\dot{\alpha} r$$
$$= m_f\omega\dot{r} + (D + B_2 r^2)\frac{\omega}{2} r + F_{bT}, \tag{7.3}$$

with $m_a = m + m_f$. This fourth-order system can be transformed into a third-order system with the whirl velocity $\Omega = \dot{\alpha}$,

$$m_a(\ddot{r} - \Omega^2 r) + (c + D + B_2 r^2)\dot{r} + \left(k - \frac{\omega^2}{4} m_f + m_f\omega\Omega + B_1 r^2\right)r$$
$$= -F_{bN}$$
$$m_a(\dot{\Omega} r + 2\dot{r}\Omega) + (c + D + B_2 r^2)\Omega r$$
$$= m_f\omega\dot{r} + (D + B_2 r^2)\frac{\omega}{2} r + F_{bT}. \tag{7.4}$$

7.2 Equilibrium Without Contact. The equilibrium without contact (r_e, Ω_e) of Eq. (7.4) has to obey $\dot{r} = \ddot{r} = \dot{\Omega} = 0$ and $r < R_c$. The whirl velocity can be derived from the second equation of Eq. (7.4),

$$\Omega_e = \frac{D + B_2 r_e^2}{c + D + B_2 r_e^2} \frac{\omega}{2}. \tag{7.5}$$

Consequently, the rotor is whirling forward in the equilibrium without contact. The first equation of Eq. (7.4) gives

$$\left(k - \frac{\omega^2}{4} m_f + m_f \omega \Omega_e - m_a \Omega_e^2 + B_1 r_e^2\right) r_e = 0. \tag{7.6}$$

Solving the latter equation gives two equilibrium branches of the system without contact. The first branch is the trivial solution

$$r_e = 0, \tag{7.7}$$

and the second branch can be derived from

$$k - \frac{\omega^2}{4} m_f + m_f \omega \Omega_e - m_a \Omega_e^2 + B_1 r_e^2 = 0. \tag{7.8}$$

The trivial branch becomes unstable when it meets the second branch. We denote the frequency at which the trivial branch becomes unstable by ω_c. Substitution of Eqs. (7.5) and (7.7) into Eq. (7.8) gives ω_c

$$\omega_c^2 = 4k \frac{(c+D)^2}{c^2 m_f + D^2 m}. \tag{7.9}$$

Two limiting cases are of special interest: a) $c > 0$ and $D = B_2 = 0$, b) $c = 0$ and $D > 0$, $B_2 > 0$.

Case (a) implies that we consider the system to rotate in a frictionless fluid. The rotor will not whirl due to the absence of fluid friction,

$$\Omega_{e,a} = 0. \tag{7.10}$$

The quasi-static motion of the rotor gives

$$c\dot{r}_{e,a} = \left(\frac{\omega^2}{4} m_f - k\right) r_{e,a} - B_1 r_{e,a}^3. \tag{7.11}$$

The two stationary solutions (for $r_{e,a} \geq 0$) are

$$r_{e,a} = 0, \quad r_{e,a} = \sqrt{\frac{\frac{\omega^2}{4} m_f - k}{B_1}} \tag{7.12}$$

We conclude that case a) gives a supercritical pitchfork bifurcation $(B_1 > 0)$ at

$$\omega_{c,a} = 2\sqrt{\frac{k}{m_f}} \tag{7.13}$$

Case (b) implies that we consider the system to have no structural damping but only fluid damping. The rotor will whirl with half the rotation speed $(1/2\omega$-whirl),

$$\Omega_{e,b} = \frac{1}{2}\omega. \tag{7.14}$$

The quasi-static motion of rotor gives (with $m_a = m + m_f$)

$$(D + B_2 r_{e,b}^2)\dot{r}_{e,b} = \left(\frac{\omega^2}{4} m - k\right) r_{e,b} - B_1 r_{e,b}^3. \tag{7.15}$$

The two stationary solutions (for $r_{e,b} \geq 0$) are

$$r_{e,b} = 0, \quad r_{e,b} = \sqrt{\frac{\frac{\omega^2}{4} m - k}{B_1}}. \tag{7.16}$$
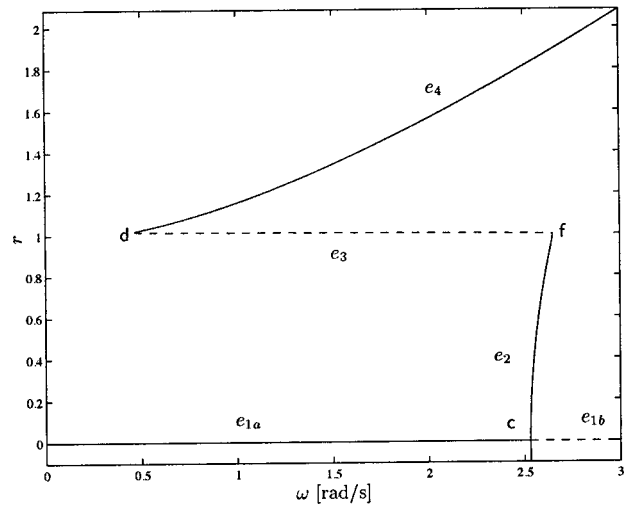

Fig. 6   Whirl Model, equilibrium branches

We conclude that case (b) also gives a supercritical pitchfork bifurcation at twice the natural frequency,

$$\omega_{c,b} = 2\sqrt{\frac{k}{m}}. \tag{7.17}$$

For $m_f/m < 1$ it can be shown that $\omega_{c,b} < \omega_c < \omega_{c,a}$. The pitchfork bifurcation is shown in Fig. 6 for the parameter values given in Appendix C. The trivial branch e_{1a} is stable and meets the bifurcation (denoted by c) after which it is unstable and continues as e_{1b}. From the bifurcation point starts a branch of stable forward whirl solutions e_2.

7.3   Equilibrium With Pure Rolling. The rotor rolls over the stator wall without slipping under three conditions:

1. the relative velocity is zero, $v_{\text{rel}} = \Omega r + \omega R = 0$,
2. positive normal contact force, $F_{bN} > 0$,
3. the tangential contact force does not exceed the maximal friction force, $-\mu_b F_{bN} \leq F_{bT} \leq \mu_b F_{bN}$.

The pure rolling equilibrium $(r = r_p, \Omega = \Omega_p)$ has to obey $\dot{r} = \ddot{r} = \dot{\Omega} = 0$.

The whirl velocity can be derived from condition 1,

$$\Omega_p = -\frac{R}{r_p}\omega. \tag{7.18}$$

Consequently, the rotor rolls backward over the stator wall. The equilibrium conditions give

$$-m_a \Omega_p^2 r_p + \left(k - \frac{\omega^2}{4} m_f + m_f \omega \Omega_p + B_1 r_p^2\right) r_p$$

$$= -F_{bN} = -k_b(r_p - R_c) \tag{7.19}$$

and

$$(c + D + B_2 r_p^2)\Omega_p r_p = (D + B_2 r_p^2)\frac{\omega}{2} r_p + F_{bT}. \tag{7.20}$$

Substitution of Ω_p in Eq. (7.19) gives a third-order polynomial in r_p. If we neglect the nonlinear fluid term B_1, Eq. (7.19) reduces to a second-order polynomial

$$\left(k + k_b - \frac{\omega^2}{4} m_f\right) r_p^2 - (k_b R_c + m_f \omega^2 R) r_p - m_a \omega^2 R^2 = 0. \tag{7.21}$$

Solving for r_p gives two roots of which only one fulfills condition 1,

$$r_p = \frac{k_b R_c + m_f \omega^2 R + \sqrt{(k_b R_c + m_f \omega^2 R)^2 + 4 m_a \omega^2 R^2 \left(k + k_b - \frac{\omega^2}{4} m_f\right)}}{2\left(k + k_b - \frac{\omega^2}{4} m_f\right)}. \qquad (7.22)$$

The limit of k_b to infinity gives of course $\lim_{k_b \to \infty} r_p = R_c$.

If we assume directly an infinitely stiff wall of the stator without neglecting B_1, then we can solve for the contact forces,

$$F_{bN} = m_a \omega^2 \frac{R^2}{R_c} - \left(k - \frac{\omega^2}{4} m_f + B_1 R_c^2\right) R_c + \omega^2 R m_f, \quad (7.23)$$

$$F_{bT} = -(c + D + B_2 R_c^2) \omega R - (D + B_2 R_c^2) \frac{\omega}{2} R_c. \quad (7.24)$$

Equation (7.23) should fulfill condition 2,

$$\omega^2 > \omega_b^2 = \frac{(k + B_1 R_c^2) R_c}{m_a \frac{R^2}{R_c} + m_f \frac{1}{4} R_c + m_f R}. \qquad (7.25)$$

If B_1 is not too large, then $\omega_b < \omega_{c,b}$.

However, pure rolling near $\omega = \omega_b$ is not possible because Eq. (7.24) has to fulfill condition 3. We define that condition 3 is violated at $\omega = \omega_d$. Substitution of Eqs. (7.23) and (7.24) into $-\mu_b F_{bN} = F_{bT}$ gives a second-order polynomial in ω_d,

$$-\mu_b \left(m_a \frac{R^2}{R_c} + m_f \left(\frac{R_c}{4} + R\right)\right) \omega_d^2$$

$$+ \left(cR + (D + B_2 R_c^2)\left(R + \frac{R_c}{2}\right)\right) \omega_d + \mu_b R_c (k + B_1 R_c^2) = 0. \qquad (7.26)$$

If the fluid damping (D, B_2) and structural damping (c) are small compared to the dry friction caused by μ_b, then we can make the following approximation

$$\omega_d^2 \approx \omega_b^2 + \frac{cR + (D + B_2 R_c^2)\left(R + \frac{R_c}{2}\right)}{\mu_b \left(m_a \frac{R^2}{R_c} + m_f \left(\frac{R_c}{4} + R\right)\right)} \omega_b. \qquad (7.27)$$

Fluid damping and structural damping cause that $\omega_d > \omega_b$.

The pure rolling branch for the parameter values of Appendix C is depicted in Fig. 6 as branch e_4. The point at which the branch stops ($\omega = \omega_d$) is denoted by d. The value R_c is taken as unity. A larger value for the borehole stiffness k_b will cause the pure rolling branch to come closer to $r = R_c$.

Branch e_2, with stable *forward* whirling solutions without contact, is connected to branch e_4, with stable *backward* whirling pure rolling solutions, by the unstable branch e_3. Branch e_3 consists of equilibria with slipping contact.

7.4 Equilibrium With Slipping Contact. The relative velocity $v_{\rm rel}$ between rotor and stator is positive for forward whirling solutions without contact (branch e_2), whereas it is zero for pure rolling solutions (branch e_4). The relative velocity during slipping contact (branch e_3) should be in between. There are two conditions for slipping:

1. the relative velocity is positive, $v_{\rm rel} = \Omega r + \omega R > 0$,
2. positive normal contact force, $F_{bN} > 0$.

The slipping equilibrium ($r = r_s$, $\Omega = \Omega_s$) has to obey $\dot{r} = \ddot{r} = \dot{\Omega} = 0$. The equilibrium conditions give

$$-m_a \Omega_s^2 r_s + \left(k - \frac{\omega^2}{4} m_f + m_f \omega \Omega_s + B_1 r_s^2\right) r_s = -F_{bN}, \qquad (7.28)$$

$$(c + D + B_2 r_s^2) \Omega_s r_s = (D + B_2 r_s^2) \frac{\omega}{2} r_s - \mu_b F_{bN}, \quad (7.29)$$

where $F_{bN} = k_b(r_s - R_c)$. This system of equations can be solved to give r_s, which will not be done in this section. The insight can be gained from other considerations. The limit of k_b to infinity gives of course

$$\lim_{k_b \to \infty} r_s = R_c.$$

The branch of slipping equilibrium begins at the point where the equilibrium without contact touches the stator wall $r_e = R_c$ (denoted by f in Fig. 6) and the branch ends at the point where the pure rolling branch begins (point d). Consequently, the slipping branch connects the stable no-contact branch to the stable pure rolling branch. Of much interest is to know *how* the slipping branch is located between the two end-points, which is closely related to its stability. We therefore try to find an expression for $\partial r / \partial \omega$ at the point where the slipping branch and the no-contact branch e_2 connect. To simplify the results we will assume $B_2 = 0$. At the connection point to the no-contact branch we have at $r_s = r_e = R_c$. The following equations hold at this point

$$\Omega_s = \Omega_e = \frac{D}{c + D} \frac{\omega}{2}, \qquad (7.30)$$

$$\left(k - \frac{\omega^2}{4} m_f + m_f \omega \Omega_e - m_a \Omega_e^2 + B_1 R_c^2\right) R_c = 0. \qquad (7.31)$$

We now differentiate Eq. (7.28) with respect to ω. This gives

$$-2 m_a \Omega_s \frac{\partial \Omega_s}{\partial \omega} r_s - m_a \Omega_s^2 \frac{\partial r_s}{\partial \omega} + \left(k - \frac{\omega^2}{4} m_f + m_f \omega \Omega_s + B_1 r_s^2\right) \frac{\partial r_s}{\partial \omega}$$

$$+ \left(-\frac{\omega}{2} m_f + m_f \Omega_s + m_f \omega \frac{\partial \Omega_s}{\partial \omega} + 2 B_1 r_s \frac{\partial r_s}{\partial \omega}\right) r_s = -k_b \frac{\partial r_s}{\partial \omega} \qquad (7.32)$$

and when we substitute Eqs. (7.30) and (7.31),

$$-m_a \frac{D}{c + D} \omega \frac{\partial \Omega_s}{\partial \omega} R_c + \left(-\frac{1}{2} + \frac{1}{2} \frac{D}{c + D} + \frac{\partial \Omega_s}{\partial \omega}\right) m_f \omega R_c$$

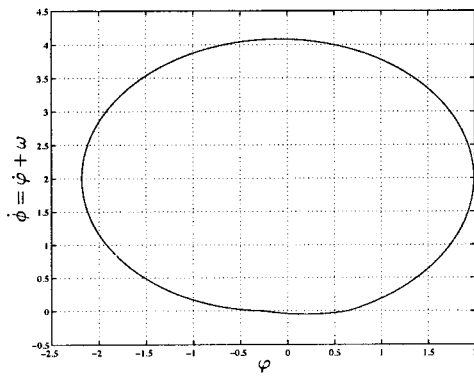$$= -(2 B_1 R_c^2 + k_b) \frac{\partial r_s}{\partial \omega}. \qquad (7.33)$$

Differentiating Eq. (7.29) gives

$$\frac{\partial \Omega_s}{\partial \omega} r_s + \Omega_s \frac{\partial r_s}{\partial \omega} = \frac{1}{2} \frac{D}{c + D} \left(r_s + \omega \frac{\partial r_s}{\partial \omega}\right) - \frac{\mu_b k_b}{c + D} \frac{\partial r_s}{\partial \omega}$$
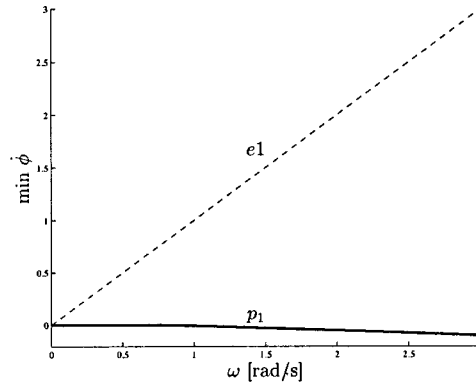
or

$$\frac{\partial \Omega_s}{\partial \omega} = \frac{1}{2} \frac{D}{c + D} - \frac{\mu_b k_b}{c + D} \frac{1}{R_c} \frac{\partial r_s}{\partial \omega}. \qquad (7.34)$$

After substitution of Eq. (7.34) in Eq. (7.33) we arrive at an expression for $\partial r_s / \partial \omega$,

(a) Periodic solution, $\omega = 2$ rad/s.

(b) Periodic branch (bold) and equilibrium branch.

Fig. 7   Stick-slip Model

$$k_b\left(1 + 2\frac{B_1}{k_b}R_c^2 - \frac{\mu_b\omega}{(c+D)^2}(m_f c - mD)\right)\frac{\partial r_s}{\partial \omega}$$

$$= \frac{1}{2}\frac{\omega R_c}{(c+D)^2}(D^2 m + c^2 m_f). \tag{7.35}$$

The limit of k_b to infinity gives of course $\lim_{k_b \to \infty} \partial r_s / \partial \omega = 0$. Two limiting cases are of special interest:

Case (a) $c > 0$, $D = 0$ and $k_b \gg B_1 R_c^2$

After substitution in Eq. (7.35) we obtain

$$k_b\left(1 - \frac{\mu_b\omega m_f}{c}\right)\frac{\partial r_s}{\partial \omega} = \frac{1}{2}\omega R_c m_f. \tag{7.36}$$

Consequently, when

$$\frac{\mu_b\omega m_f}{c} > 1 \Rightarrow \frac{\partial r}{\partial \omega} < 0,$$

$$\frac{\mu_b\omega m_f}{c} < 1 \Rightarrow \frac{\partial r}{\partial \omega} > 0.$$

Case (b) $c = 0$, $D > 0$ and $k_b \gg B_1 R_c^2$

After substitution in Eq. (7.35) we obtain

$$k_b\left(1 + \frac{\mu_b\omega m}{D}\right)\frac{\partial r_s}{\partial \omega} = \frac{1}{2}\omega R_c m. \tag{7.37}$$

Consequently, it must hold that $\partial r / \partial \omega > 0$.

The parameter values of the structural damping and fluid damping are $c = 0.3$ N/(ms) and $D = 0.1$ N/(ms). The numerical example is similar to case (a) with $\mu_b\omega m_f / c > 1$. The derivative $\partial r / \partial \omega$ at point f is therefore negative which causes the branch e_3 to be unstable and to connect point d with point f directly. If the parameter values would be different, such that $\mu_b\omega m_f / c < 1$, then branch e_3 would start at point f with a positive slope as a stable branch. It will at some point turn around and continue as an unstable branch in the direction of point d.

Bifurcation points d and f are discontinuous saddle-node bifurcations of the equilibrium branch $e_2 - e_3 - e_4$. An eigenvalue jumps over the imaginary axis through the origin at those bifurcation points. At bifurcation point d, being the transition from contact to no-contact, this is caused by the non-smoothness of the normal contact force Eq. (6.1). At bifurcation point f, being the transition from slip to stick, this is caused by the non-smoothness of the tangential contact force, Eq. (6.2). Remark the angle between the branches at a discontinuous bifurcation point.

8   Stick-Slip Model

In this section we study only the Stick-slip Model. We assume the rotor to rotate concentrically in the stator (no lateral vibration, $r = 0$). As there is no radial displacement, the torques due to fluid forces and contact forces vanish ($T_d = 0$, $T_b = 0$). The equation of motion for pure torsional motion is

$$J\ddot{\varphi} = -k_\varphi\varphi + T_f. \tag{8.1}$$

The Stick-slip Model has an unstable equilibrium branch ($\varphi = T_f(\omega)/k$, $\dot{\varphi} = 0$), which corresponds to the trivial equilibrium branch ($r = 0$, $\varphi = T_f(\omega)/k$) of the full Stick-slip Whirl Model. The trivial equilibrium branch was denoted in the Whirl Model as branch e_1 (Fig. 6).

8.1   Periodic Stick-Slip Vibrations.   The periodic solutions of the Stick-slip Model are also periodic solutions of the Stick-slip Whirl Model (compare Eq. (8.1) with Eq. (9.1) for $r = T_b = T_d = 0$). The periodic stick-slip vibration is depicted in Fig. 7(a). The twist φ is on the horizontal axis and the angular velocity $\dot{\phi} = \dot{\varphi} + \omega$ on the vertical axis. The limit cycle is traversed clock-wise. The slip part of the motion takes place at $\dot{\phi} > 0$. When the velocity is decreasing during the slip part, it arrives at $\dot{\phi} = 0$ and continues with backward rotation ($\dot{\phi} < 0$). This backward slip motion is followed by the stick part $\dot{\phi} = 0$, which completes the limit cycle.

The branch of periodic stick-slip solutions (p_1) is numerically determined for varying values of ω and depicted in Fig. 7(b). The minimal value of $\dot{\phi}$ is set on the vertical axis. For the trivial equilibrium branch holds min $\dot{\phi} = \omega$ and this branch is unstable as the friction torque T_f decreases with increasing angular velocity $\dot{\phi}$. The periodic stick-slip branch has a minimal value of $\dot{\phi}$, being smaller or equal than zero depending on the backward slip part. As can be seen from Fig. 7(b), backward rotation becomes more pronounced at higher values of ω.

9   Stick-Slip Whirl Model

The Stick-slip Model and the Whirl Model will be combined in this section which gives the Stick-slip Whirl Model.

9.1   Equations of Motion.   Combining the lateral and the torsional model and taking into account the nonstationary fluid forces, fluid torque and contact torque (Section 6.1) gives the following set of equations of motion
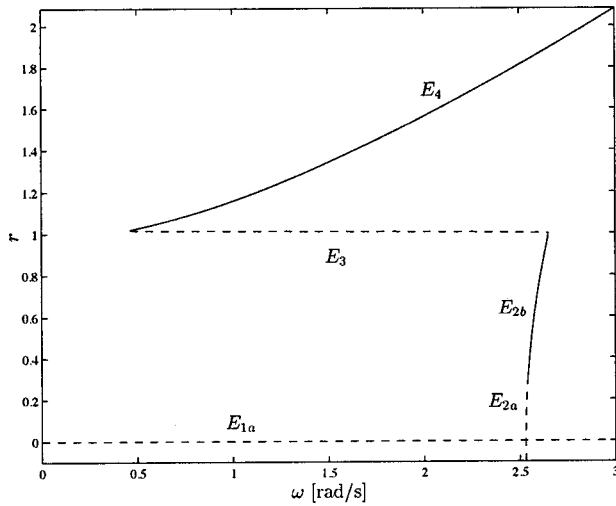
Fig. 8 Stick-slip Whirl Model, equilibrium branches

Fig. 10 Stick-slip Whirl Model, zoom of Fig. 9

$$m_a(\ddot{r}-\Omega^2 r)+(c+D+B_2 r^2)\dot{r}+\left(k-\frac{\dot{\phi}^2}{4}m_f+m_f\dot{\phi}\Omega+B_1 r^2\right)r$$

$$=-F_{bN}$$

$$m_a(\dot{\Omega}r+2\dot{r}\Omega)+(c+D+B_2 r^2)\Omega r$$

$$=m_f\dot{\phi}\dot{r}+(D+B_2 r^2)\frac{\dot{\phi}}{2}r+F_{bT} \qquad (9.1)$$

$$J\ddot{\varphi}=-k_\varphi\varphi+T_f+T_b+T_d .$$

9.2 Equilibrium Branches. Equilibrium positions of sub-models are in general not equilibrium positions of the total model. The torsional and lateral degrees of freedom of the Stick-slip Whirl Model however, are to some extent uncoupled. From Eq. (9.1) it follows that for an equilibrium position must hold that $\dot{r}=0$, $\dot{\Omega}=0$ and $\dot{\varphi}=0$. The angular velocity of the rotor is therefore constant, $\dot{\phi}=\omega$, which means that the Whirl Model is not influenced by the Stick-slip Model. The equilibrium branches e_1 to e_4 of the Whirl Model are also equilibrium branches of the Stick-slip Whirl Model, denoted by E_1 to E_4 (Fig. 8). The twist angle $\varphi_{\rm eq}$ in an equilibrium position can be found from substitution of an equilibrium position of the Whirl Model $r_{\rm eq}$ and $\Omega_{\rm eq}$ in
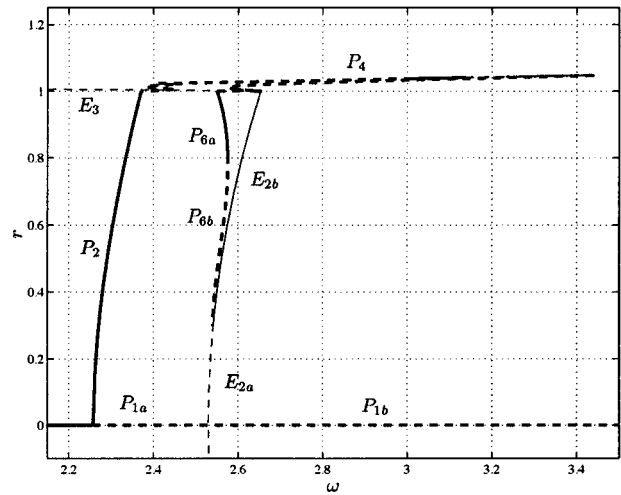
$$k_\varphi\varphi_{\rm eq}=T_f(\omega)+T_b(\Omega_{\rm eq},\omega,r_{\rm eq})+T_d(\Omega_{\rm eq},\omega,r_{\rm eq}). \qquad (9.2)$$

Some stable branches may become unstable due to an added eigenvalue of the Stick-slip Model. The trivial branch E_1 of the Stick-slip Whirl Model is totally unstable whereas it was partly stable for the Whirl Model. At the bifurcation point of branch E_1, a second eigenvalue enters the right half-plane, which explains why the branch does not exchange stability at the bifurcation point. The branch E_2 contains a Hopf bifurcation which splits the branch in a stable and an unstable part.

9.3 Periodic Branches. The periodic branches of the Stick-slip Whirl Model are depicted in Fig. 9 and partly enlarged in Figures 10, 11, and 12.

As for equilibrium positions, periodic solutions of submodels are in general not periodic solutions of the total model. The torsional and lateral degrees of freedom of the Stick-slip Whirl Model are however uncoupled for $r=0$ (because T_d and T_b vanish). The Whirl Model has an equilibrium position $r=0$. Branch p_1 of the Stick-slip Model (Section 8) therefore also exists for the Stick-slip Whirl Model as branch P_1 with $r=0$. Whereas branch p_1 is stable, branch P_1 is partly stable due to the added eigenvalues of the Whirl Model.

Branch P_1 consist of pure stick-slip vibrations with $x=0$ and $y=0$. The radial deflection is therefore $r=\sqrt{x^2+y^2}=0$ but the angular position $\alpha=\arctan(y/x)$ is not defined. Branch P_1 can
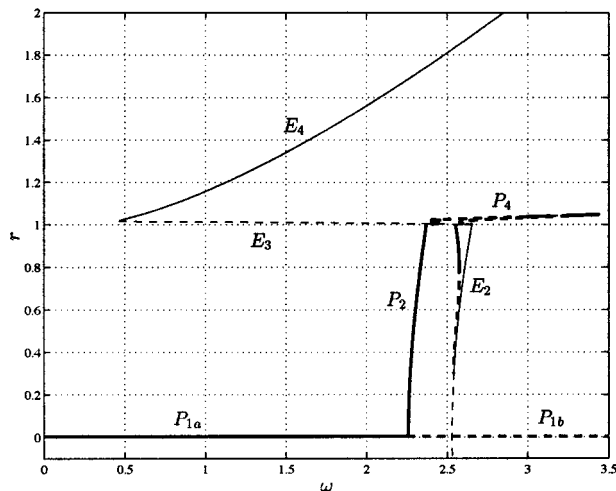

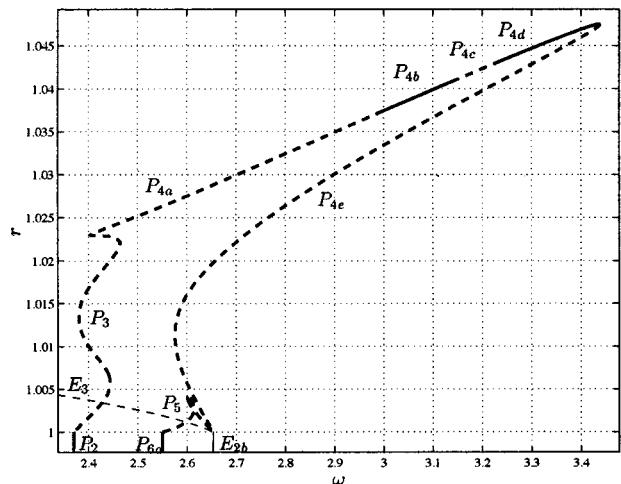
Fig. 9 Stick-slip Whirl Model, periodic branches (bold)
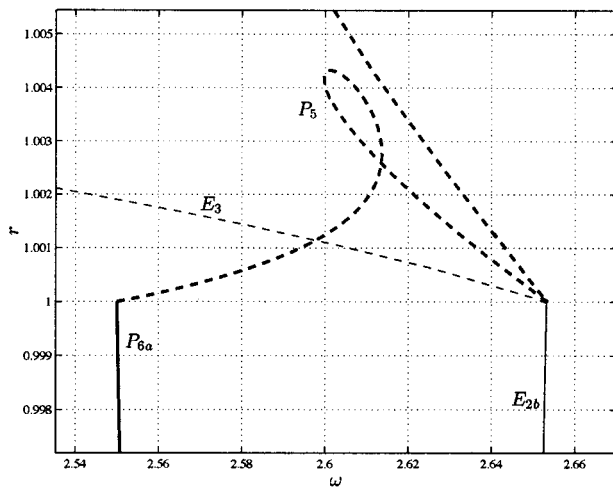

Fig. 11 Stick-slip Whirl Model, zoom of Fig. 10

Fig. 12 Stick-slip Whirl Model, zoom of Fig. 11

therefore only be described in the stationary coordinate system (x, y, φ) and not in the polar coordinate system (r, α, φ), which was used for the Whirl Model.

Branch P_1, described in the stationary coordinate system, contains a Neimark-Sacker (or secondary Hopf) bifurcation after which the branch is unstable.

The equilibrium branches E_2 to E_4 (which are pure whirl solutions) and the pure stick-slip branch P_1 both have a bifurcation point in the Stick-slip Whirl Model which was not existing in Stick-slip or Whirl Model. The equilibrium branches E_2 to E_4 contain equilibria in polar coordinates but are periodic solutions in stationary coordinates with period times $T = 2\pi/\omega$. From the Hopf bifurcation on E_2 emanates a branch P_6 (Fig. 10), which is periodic in polar coordinates and quasi-periodic in stationary coordinates. Branch P_6 is connected through branches P_5, P_4 and P_3 with branch P_2 (Fig. 11). Branch P_2, which contains periodic solutions in polar coordinates and quasi-periodic solutions in stationary coordinates, ends at the Neimark-Sacker bifurcation on P_1. The Neimark-Sacker bifurcation therefore gives rise to quasi-periodic solutions which is consistent with the theory.

Branches P_2 to P_6 connect the solutions found from the Whirl Model with the solutions found from the Stick-slip Model. Branches P_2 and P_3 are periodic solutions (in polar coordinates) that perform both stick-slip and whirl motion. The periodic solutions on branches P_3, P_4 and P_5 contains contact events between the rotor and the stator wall.

Branch P_4 is divided in stable and unstable parts P_{4a} to P_{4d}. Branch P_{4a} is connected to P_{4b} by a Neimark-Sacker bifurcation. Branches P_{4b}, P_{4c} and P_{4d} are connected to each other by two flip bifurcations. The branches with period-doubled periodic solutions and quasi-periodic solutions, which start at these bifurcations, have not been calculated.

A number of discontinuous bifurcations exist on the branches P_2 to P_6. Branch P_2 is connected to P_3 (Fig. 12) by a discontinuous flip bifurcation (the period-doubled branch has not been calculated). The bifurcation occurs when the periodic solution touches the stator, $r = R_c$. The discontinuity of the contact forces causes the discontinuous bifurcation. Similarly, branch P_5 is connected to branch P_6 (Fig. 12) by a discontinuous fold bifurcation at $r = R_c$. Branch P_3 (with stick events) is connected to branch P_4 (without stick events) by a discontinuous fold bifurcation. This bifurcation is due to the discontinuity in the dry friction force.

A remarkable bifurcation occurs on the equilibrium branch connecting branch E_{2b} with E_3 at $r = R_c$ (Fig. 12). This bifurcation point was already encountered in the Whirl Model as a discontinuous saddle-node bifurcation at which the branch turns around (bifurcation point f in Fig. 6). In addition, two periodic branches,

P_4 and P_5, are connected to the bifurcation point in the Stick-slip Whirl Model. This bifurcation point is therefore a combined bifurcation of a saddle-node bifurcation and two Hopf bifurcations.

The bifurcation diagrams certainly do not show all periodic branches that exist. Period-doubled branches were not calculated but also other branches may be missing in the bifurcation diagrams.

A note has to be made concerning the chosen numerical values of the parameters in the Stick-slip Whirl Model. Stiffness and mass/inertia parameters are chosen such that the torsional eigenfrequency of the rotor is close to the first torsional eigenfrequency of the drillstring. Similarly, the lateral eigenfrequency of the rotor is close to the lateral eigenfrequency of the lowest drill collar section. Damping and friction constants are more or less arbitrarily chosen. The equilibrium and periodic branches in the bifurcation diagrams depend of course on the chosen constants. However, the periodic whirl branches, P_2 to P_6, seem to be close to the equilibrium branch E_2. The equilibrium branches form a structure to which the periodic branches are attached. A lot about the dynamics of this particular system can already be said once the location of the equilibrium branches are known. The value ω_c, expressed in Eqs. (7.13) and (7.17), gives the location of branch E_2. The ratio $\mu_b \omega m_f / c$ determines whether branch E_3 proceeds to the right of bifurcation point f or folds to the left (Fig. 6). The value ω_d of Eq. (7.27) gives the starting point of branch E_4. Consequently, ω_c, ω_d and $\mu_b \omega m_f / c$ determine the main structure of the bifurcation diagram.

10 Discussion and Conclusions

In the previous sections a simple model was constructed, based on the assumption that the fluid forces are the cause of the phenomena observed in the measurements. The Stick-slip Whirl Model was analyzed with path-following techniques and bifurcation theory presented in [15,16]. What can we conclude from the Stick-slip Whirl Model with respect to the measurements?

The Stick-slip Whirl Model exhibits both stick-slip motion and whirl motion (which is not possible in the models of Jansen [2]). Stick-slip motion is prevalent at low angular velocities and backward whirl (during which the rotor rolls backward over the stator) is prevalent for high angular velocities consistent with the measurements. Stick-slip and whirl motion coexist for an interval of ω both in the model and in the measurements. Combined stick-slip whirl motion was not observed in the measurements but was found in the Stick-slip Whirl Model (branches P_2 and P_3). However, this combined motion occurs only in a very small interval of ω in the model. The model is therefore consistent with the measurements in the sense that stick-slip motion occurs *or* whirl motion (both possible for the same value of ω), but a combination is rare or not existing.

The measurements show a hysteresis effect for a sweep-up sweep-down test (Fig. 4). The drillstring starts in stick-slip motion at low angular velocity of the rotary table. When the rotary table speed is increased with small steps, the motion remains in the stick-slip mode but at 11.5 [rad/s] the drillstring suddenly stops to operate in the stick-slip mode and starts to whirl backward. The drillstring remains whirling for increasing rotary table speed also after the rotary table speed is diminished in small steps during the sweep-down test. The mean-bending moment (and whirl radius?) drop between 7 and 2 [rad/s] and stick-slip recommences.

A similar hysteresis effect can be seen for the Stick-slip Whirl Model. At low values of ω the rotor is in stick-slip motion. When ω is increased quasi-statically, branch P_{1a} is followed (Fig. 9) and the rotor will remain in the stick-slip mode. Branch P_1 becomes unstable for increasing ω due to the destabilizing fluid forces and the motion of the rotor will rapidly change via branches P_2 and P_3 to an oscillatory whirl motion on branch P_4. When ω is increased even more the motion will jump to regular backward whirling motion without slip on branch E_4. If ω is subsequently quasi-statically decreased, the rotor will remain to operate on

branch E_4 until the discontinuous saddle-node bifurcation between E_3 and E_4 is met. The motion will then jump to the stick-slip mode and the hysteresis loop is complete.

The phenomena as described by the Stick-slip Whirl Model resemble to some extent the phenomena observed in the measurements. The transition from stick-slip motion to whirl motion is similar, but the transition from whirl to stick-slip motion seems to be more gradual in the measurements than can be explained from the model.

One could argue whether the observed phenomena in the measurements are really due to fluid forces and not to other possible ways of interaction between torsional and lateral motion. Although the results on the Stick-slip Model look similar, they do not prove that indeed fluid forces are the cause for onset of whirl in drillstrings. This paper illustrates how the techniques and theory of [15,16] can be used to analyze low-dimensional models with discontinuities, in this case the Stick-slip Whirl Model. In the same way, other low-dimensional models can be constructed which study for instance the influence of mass unbalance on the dynamic behavior of a rotor with lateral and torsional degrees of freedom. The results of the different models can be compared with the experiments which can help to gain insight into the complex dynamic behavior of the drillstring. Knowledge about bifurcations in discontinuous systems is therefore relevant to dynamic problems in industrial applications.

Acknowledgment

Appendix A: Discontinuous Bifurcations

Physical phenomena such as dry friction, impact and backlash in mechanical systems or diode elements in electrical circuits are often studied by means of mathematical models with some kind of discontinuity. Filippov systems [22,23] form a subclass of discontinuous dynamical systems which can be described by a set of first-order ordinary differential equations with a discontinuous right-hand side, e.g.

$$\dot{\underline{x}}(t) = \underline{f}(t,\underline{x}(t)) = \begin{cases} \underline{f}_-(t,\underline{x}(t)) & \underline{x} \in \mathcal{V}_- \\ \underline{f}_+(t,\underline{x}(t)) & \underline{x} \in \mathcal{V}_+ \end{cases}, \qquad (10.1)$$

where the right-hand side $\underline{f}(t,\underline{x})$ is assumed to be discontinuous but such that it is piecewise continuous and smooth on $\mathcal{V}_-$ and $\mathcal{V}_+$ and discontinuous on the hyperplane Σ, being the border between $\mathcal{V}_-$ and $\mathcal{V}_+$.

Mechanical systems with dry friction constitute an important example of Filippov systems [24]. The presence of dry friction-induced self-sustained vibrations can be highly detrimental to the performance of mechanical systems, like for the drillstring problem discussed in this paper. Many other practical problems in engineering are related to vibrations caused or influenced by discontinuous characteristics of physical phenomena. It is therefore desirable to know whether periodic solutions of a system with dry friction (or Filippov systems in general) exist for a certain parameter set and how these periodic solutions change for a varying parameter of the system. Such parameter studies are usually conducted by means of path-following techniques where a branch of fixed points or periodic solutions is followed while varying a parameter. A branch of fixed points or periodic solutions can fold or can split into other branches at critical parameter values (Fig. 13(a)). This qualitative change in the structural behavior of the system is called 'bifurcation'. Bifurcations in smooth systems are well understood but little is known about bifurcations in non-smooth and discontinuous systems. It is shown in [16] that a bifurcation in a non-smooth continuous system can be discontinuous in the sense that an eigenvalue jumps over the imaginary axis under the variation of a parameter (Fig. 13(b)).

In [16] different aspects were investigated of bifurcations of fixed points in non-smooth continuous systems and of periodic solutions in Filippov systems (see also [25]). The Poincaré map relates the bifurcations of fixed points in non-smooth continuous systems to bifurcations of periodic solutions in Filippov systems. Filippov systems expose nonconventional bifurcations called ''discontinuous bifurcations'', being different from the conventional bifurcations occurring in smooth systems. Filippov theory, generalized derivatives and Floquet theory were combined in [16], which leads to new insight into bifurcations in discontinuous systems.

The theory of Filippov gives a solution concept for differential equations with discontinuous right-hand side. Differential equations with discontinuous right-hand side are extended to differential inclusions with Filippov's convex method. Existence of solutions to differential inclusions is guaranteed under additional conditions but no uniqueness of solutions is guaranteed. Nonuniqueness plays an important role in the bifurcation behavior of Filippov systems.

The local stability of a periodic solution is governed (for the hyperbolic case) by the fundamental solution matrix $\Phi(T + t_0, t_0)$, which can be obtained for smooth systems from the initial value problem

$$\dot{\Phi}(t,t_0) = \frac{\partial \underline{f}(t,\underline{x}(t))}{\partial \underline{x}} \Phi(t,t_0), \quad \Phi(t_0,t_0) = \Phi_0 = \underline{I}.$$

The fundamental solution matrix is also essential for the understanding of bifurcations of periodic solutions. Discontinuities of the vector field in Filippov systems cause jumps in the fundamental solution matrix.

The jumps in the fundamental solution matrix can be analyzed by the linear approximation method which approximates a discon-
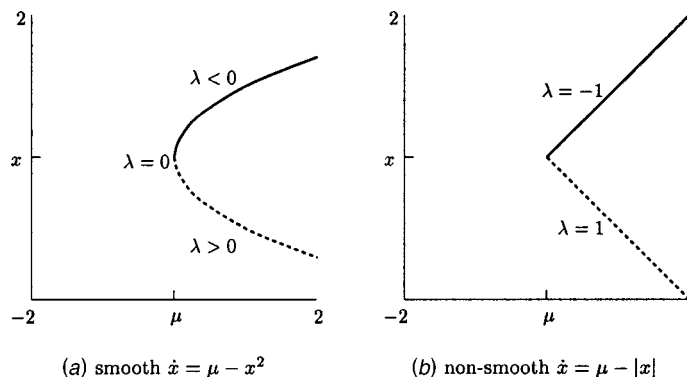

(a) smooth $\dot{x} = \mu - x^2$ (b) non-smooth $\dot{x} = \mu - |x|$

Fig. 13   Saddle-node bifurcation in a smooth and non-smooth system

tinuous system by a non-smooth continuous system. The linear approximation method replaces a discontinuity in the vector field by a boundary layer with a vector field that varies linearly between the left and right limit on the edges of the boundary layer. It is found that the jump of the fundamental solution matrix can be expressed as a convex combination of the fundamental solution matrices before and after the jump

$$\widetilde{\Phi} = \{(1-q)\Phi_- + q\Phi_+ , \forall 0 \leq q \leq 1\},$$

where Φ_- and Φ_+ denote the fundamental solution matrix before and after the jump respectively. Different definitions for the term bifurcation exist in literature and it is shown in [16] that they can be inconsistent with one another for Filippov systems. The definition of Seydel [26], which is applicable to Filippov systems, has been chosen in this paper as definition for bifurcation.

Branches of periodic solutions in Filippov systems expose discontinuous bifurcations similar to discontinuous bifurcations of fixed points in non-smooth continuous systems. The basic idea is that Floquet multipliers (eigenvalues of the fundamental solution matrix) of periodic solutions in Filippov systems can jump when a parameter of the system is varied. Such a jump can occur if a periodic solution becomes tangential to the tip of a non-smooth hyper-surface on which the vector field is discontinuous. If a Floquet multiplier jumps over the unit circle in the complex plane, a discontinuous bifurcation is encountered.

The model system of a drillstring describing whirl and stick-slip, which is studied in Section 9, belongs to the class of Filippov systems and exhibits several types of discontinuous bifurcations.

Appendix B: Coordinate Systems

$$x = r \cos \alpha \tag{10.2}$$
$$y = r \sin \alpha$$

$$r = \sqrt{x^2 + y^2} \quad \alpha = \arctan\left(\frac{y}{x}\right) \tag{10.3}$$

$$\dot{r} = \frac{x\dot{x} + y\dot{y}}{r} \quad \dot{\alpha} = \frac{\dot{y}x - \dot{x}y}{r^2} \tag{10.4}$$

$$\ddot{r} = \frac{\dot{x}^2 + \dot{y}^2 + \ddot{x}x + \ddot{y}y - \dot{r}^2}{r} \tag{10.5}$$

Appendix C: Parameter Values

$$m = 1 \text{ kg} \quad c = 0.3 \text{ N/(ms)} \quad k = 1 \text{ N/m}$$

$$m_f = 1 \text{ kg} \quad D = 0.1 \text{ N/(ms)} \quad R = 2 \text{ m}$$

$$R_b = 3 \text{ m} \quad R_c = R_b - R = 1 \text{ m} \quad k_b = 50 \text{ N/m}$$

$$c_b = 30 \text{ N/(ms)} \quad \mu_b = 0.5 \quad B_1 = 0.1 \text{ N/m}^3$$

$$B_2 = 0 \text{ N/(m}^3 \text{ s)} \quad J = 1 \text{ kg m}^2 \quad k_\varphi = 1 \text{ Nm}$$

$$T_0 = 0.2 \text{ Nm} \quad \delta = 0.3$$

References

[1] Jansen, J. D., 1991, "Nonlinear Rotor Dynamics as Applied to Oilwell Drill-string Vibrations," J. Sound Vib., **147**(1), pp. 115–135.

[2] Jansen, J. D., 1993, "Nonlinear Dynamics of Oilwell Drillstrings," Ph.D. Thesis, Delft University Press, The Netherlands.

[3] Jansen, J. D., and Van den Steen, L., 1995, "Active Damping of Self-exited Torsional Vibrations in Oilwell Drill strings," Journal of Sound and Vibration, **179**(4), pp. 647–668.

[4] Kreuzer, E., and Kust, O., 1996, "Analyse selbsterregter Drehschwingungen in Torsionstäben," Zeitschrift für Angewandte Mathematik und Mechanik, **76**(10), pp. 547–557.

[5] Kust, O., 1998, "Selbsterregte Drehschwingungen in schlanken Torsionssträngen; Nichtlineare Dynamik und Regelung," Fortschr.-Ber. VDI Reihe **11**, Nr. 270, VDI Verlag, Düsseldorf.

[6] Van den Steen, L., 1997, "Suppressing Stick-slip-induced Drillstring Oscillations: A Hyperstability Approach," Ph.D. Thesis, University of Twente, The Netherlands.

[7] Van der Heijden, G. H. M., 1994, "Nonlinear Drillstring Dynamics," Ph.D. Thesis, University of Utrecht, The Netherlands.

[8] Brett, J. F., 1991, "The Genesis of Bit-induced Torsional Drill string Vibrations," SPE/IADC 21943, Paper presented at the SPE/IADC Drilling Conference held in Amsterdam, March 11–14, 1991.

[9] Dufeyte, M. P., and Henneuse, H, 1991, "Detection and Monitoring of the Slip-Stick Motion: Field Experiments," SPE/IADC 21945, Paper presented at the SPE/IADC Drilling Conference held in Amsterdam, March 11–14, 1991.

[10] Dykstra, M. W., Chen, D. C-K., Warren, T. M., and Zannoni, S. A., 1994, "Experimental Evaluations of Drill String Dynamics," SPE/IADC 28323, Paper presented at the 69th Annual Technical Conference and Exhibition of the Society of Petroleum Engineers held in New Orleans, September 1994, pp. 319–334.

[11] Dykstra, M. W., Chen, D. C-K., Warren, T. M., and Azar, J. J., 1995, "Drill-string Component Mass Imbalance: A Major Source of Downhole Vibrations," SPE/IADC 29350, Paper presented at the SPE/IADC Drilling Conference, Amsterdam, February 28–March 2, 1995.

[12] Pavone, D. R., and Desplans, J. P., 1994, "Application of High Sampling Rate Downhole Measurements for Analysis and Cure of Stick-Slip in Drilling," SPE 28324, Paper presented at the SPE 69th Annual Technical Conference and Exhibition held in New Orleans, September 25–28, 1994.

[13] Leine, R. I., and Van Campen, D. H., 1999, "Fold Bifurcations in Discontinuous Systems," *Proceedings of DETC'99 ASME Design Engineering Technical Conferences*, September 12–15, Las Vegas, CD-ROM, DETC99/VIB-8034.

[14] Leine, R. I., and Van Campen, D. H., 2002, "Discontinuous Bifurcations of Periodic Solutions," accepted for publication in Mathematical Modelling of Nonlinear Systems.

[15] Leine, R. I., Van Campen, D. H., and Van de Vrande, B. L., 2000, "Bifurcations in Nonlinear Discontinuous Systems," Nonlinear Dyn., **23**(2), pp. 105–164.

[16] Leine, R. I., 2000, "Bifurcations in Discontinuous Mechanical Systems of Filippov-Type," Ph.D. thesis, Eindhoven University of Technology, The Netherlands.

[17] Lee, Chong-Won, 1993, *Vibration Analysis of Rotors*, Kluwer Academic Publishing, Dordrecht.

[18] Tondl, A., 1965, *Some Problems of Rotor Dynamics*, Chapman and Hall Limited, London.

[19] Fritz, R. J., 1970, "The Effects of an Annular Fluid on the Vibrations of a Long Rotor, Part 1-Theory," ASME J. Basic Eng., **92**, pp. 923–929.

[20] Muszynska, A., 1986, "Whirl and Whip-Rotor/Bearing Stability Problems," J. Sound Vib., **110**(3), pp. 443–462.

[21] Leine, R. I., Van Campen, D. H., De Kraker, A., and Van den Steen, L., 1998, "Stick-Slip Vibrations Induced by Alternate Friction Models," Nonlinear Dyn., **16**(1), pp. 41–54.

[22] Clarke, F. H., Ledyaev, Yu. S., Stern, R. J., and Wolenski, P. R., 1998, *Nonsmooth Analysis and Control Theory*, Graduate Texts in Mathematics 178, Springer, New-York.

[23] Filippov, A. F., 1988, "Differential Equations with Discontinuous Right-Hand Sides," Mathematics and Its Applications, Kluwer Academic, Dordrecht.

[24] Brogliato, B., 1999, *Nonsmooth Mechanics*, Springer, London.

[25] Di Bernardo, M., Feigin, M. I., Hogan, S. J., and Homer, M. E., 1999, "Local Analysis of C-Bifurcations in *n*-Dimensional Piecewise-Smooth Dynamical Systems," Chaos, Solitons Fractals, **10**(11), pp. 1881–1908.

[26] Seydel, R., 1994, "Practical Bifurcation and Stability Analysis; From Equilibrium to Chaos," *Interdisciplinary Applied Mathematics 5*, Springer-Verlag, New York.